Short Communication

Electrochemical Impedance Studies on the Corrosion of Cu-35Ni-10Al Alloy in a Molten (0.62Li, 0.38K)₂CO₃ Environment

Yanjie Ren[1,2], Yucheng Peng[1,2], Jian Chen[1,2], Wei Qiu[1,2], Wei Li[1,2], Cong Li[1,2], Yan Niu[1,2**]*

[1] School of Energy and Power Engineering, Changsha University of Science &Technology, Changsha, Hunan 410114, China;
[2] Key Laboratory of Energy Efficiency and Clean Utilization, Education Department of Hunan Province, Changsha University of Science & Technology, Changsha, Hunan 410114, China
*E-mail: hncsqqwk86@126.com; YNiu_0320@163.com

Cu alloy is an anode material that can act as an alternative to Ni alloy in molten carbonate fuel cells (MCFCs) because of its thermodynamic stability in the anode gas atmosphere and its lower cost. To evaluate its potential application as an anode material for MCFCs, the high-temperature corrosion behaviour of cast Cu-35Ni-10Al alloy was studied in molten (0.62Li, 0.38K)₂CO₃ at 650°C in air by electrochemical impedance spectroscopy. An equivalent circuit is proposed to fit the impedance spectroscopy results. The values of R_t decreased with the immersion time, suggesting an enhanced corrosion rate. A porous and layered scale formed on the alloy after immersion for 48 h in the melt. Internal oxidation was observed in the Cu-rich zone of the alloy.

1. INTRODUCTION

Due to their high efficiency and low environmental pollution, molten carbonate fuel cells (MCFCs) have received much attention recently. For MCFCs, most of the anodes are composed of Ni–Cr or Ni–Al alloys[1-3]. However, nickel-based anodes are too expensive to widely promote MCFC commercialization, even though they show excellent performance. Thus, it is urgent to develop anode materials with low cost and stability to replace nickel-based alloys.

Similar to nickel, Cu has good catalytic activity for the oxidation of hydrogen. It also has a wider stability zone than nickel and is thermodynamically stable in the anode gas atmosphere. Furthermore, Cu possesses a higher electrical conductivity and greater resistance to carburization than nickel[4]. However, its electrochemical performance and sintering resistance are not as good as those of nickel.

Park[5] reported that the addition of Ni to copper could increase the electrochemical performance significantly, allowing the performance to reach the same level as that of a nickel anode. Nevertheless, its structure was less stable than that of a nickel anode. Hwang[6] demonstrated that the addition of Al could dramatically improve the sintering resistance of Cu-Ni alloys. Due to its excellent conductivity and sintering properties, a Cu-Ni-Al alloy is considered an ideal material for anodes in MCFCs.

In the working environments of MCFCs, the anodes are subjected to high temperature and compression loads simultaneously. Li[7-8] investigated the effect of the deformation temperature and loading rate on the mechanical properties of Cu-Ni-Al alloys. Because MCFC anodes must be exposed to molten carbonate at high temperature, the chemical stability of Cu-Ni-Al alloys needs further research. To date, limited data concerning the corrosion behaviour of Cu-Ni-Al alloys in molten carbonate at high temperatures are available.

Electrochemical impedance spectroscopy (EIS), which has been widely used to investigate aqueous corrosion, could provide substantial information on corrosion mechanisms. A limited number of reports on the application of impedance spectroscopy for corrosion in molten salt is available[9-13]. Ni[9] studied the initial stage corrosion of 310 stainless steel beneath a thin film of molten (0.62 Li, $0.38K)_2CO_3$ at 650°C. The impedance spectroscopy results showed a diffusion-controlled process that was related to the severe loss of molten salt. Liu[10] investigated the corrosion behaviour of pure Fe and pure Cr at 600°C under a deposit of solid NaCl by using electrochemical impedance spectroscopy. The results showed that there was a good relationship between the R_{ox}(the resistance of the oxide layer) and the reaction rate for both pure Fe and Cr with different corrosion time. Zahrani[11] also observed a diffusion-controlled process for the corrosion of the Inconel 625 superalloy in a $PbSO_4$–Pb_3O_4–$PbCl_2$–Fe_2O_3–ZnO environment in air by EIS. Zhu[12] used EIS technique to evaluate the corrosion behavior of 316 SS in molten nitrate salt and found that the corrosion processes of 316 SS at 450 °C and 600°C are controlled by outward diffusion of metal ions and oxygen vacancies, while corrosion mechanism at 680 °C changes to was controlled by the inward diffusion of oxygen ions.

Aiming to evaluate the potential application of Cu-Ni-Al alloy as the anode material of MCFCs, the corrosion behaviour of as-cast Cu-35Ni-10Al (in mass percent) alloy in molten (0.62 Li, $0.38K)_2CO_3$ is investigated by EIS.

2. MATERIALS AND METHODS

Bulk copper and nickel with 99.99% purity and bulk aluminium with 99.86% purity were used as the base materials. The copper, nickel and aluminium were placed into an intermediate frequency furnace, where the frequency is 20～40 Hz, the current is 20 A and the temperature is 1500°C, with nickel and aluminium in a proportion of 35%+10% (mass percentage) and melted for 1 h. During this period, long strips of charcoal were added to the molten metal to prevent oxidation of the alloy. Then, Cu-35Ni-10Al ingots were cast after refining and slag removal, and the actual composition of the cast Cu alloy was 56.05%Cu-34.3%Ni-9.65%Al (mass percent). As shown in Fig. 1, the bright zone (a) is a Cu-rich phase (b), and the dark zone is a Ni-Al-rich phase. In addition, there are some granular, acicular,

plum blossom-shaped Ni-rich phases in the Cu matrix (c), and some granular, needle-like, rod-like Cu-rich phases in the Ni-rich phase region (d).

A two-electrode system was used for the electrochemical impedance measurements[13]. The working electrode of Cu-35Ni-10Al was prepared as follows: samples with a diameter of 8 mm and a thickness of 2 mm were cut from the original ingot and then ground with 1200 grit SiC paper. A Fe–Cr wire was spot-welded to one end of the sample for electrical connection.
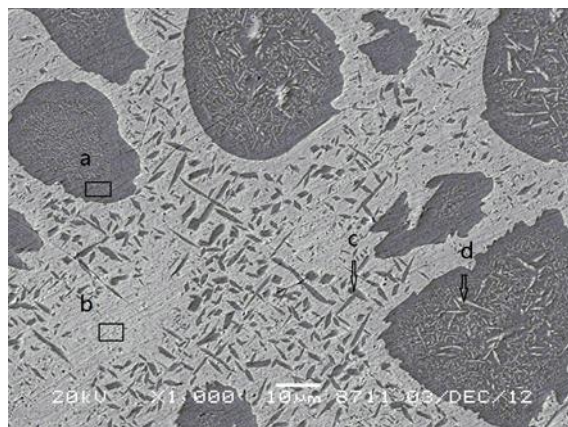

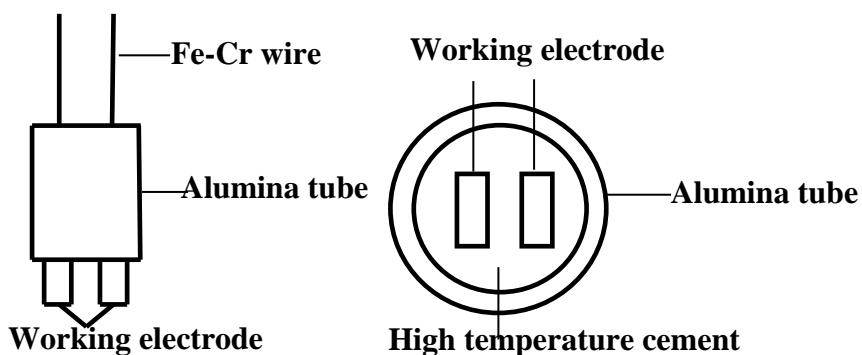**Figure 1.** SEM image of the as-cast Cu–35Ni–10Al alloy

Figure 2. Schematic diagram of the electrode arrangement.

Two closely spaced samples were sealed in an alumina tube by a high-temperature cement (as shown in Fig. 2). After the cement was dried at room temperature, it was further solidified at 200°C for 24 h. Before impedance measurements, the working electrode surface was polished again by 1000 grit SiC paper. Finally, it was degreased and dried.

A closed end and ground stainless-steel tube was used as the corrosion chamber to eliminate the effect of electric and magnetic fields caused by the furnace on the impedance measurements. A mixture of $(0.62Li, 0.38K)_2CO_3$ (mole fraction) was employed in the present study. The mixture was dried in an alumina crucible at 200°C for 24 h in air. Then, the furnace was heated to the experimental temperature of 650°C. The electrode was dipped into the melt for 48h, and electrochemical impedance spectroscopy (EIS) was used to study the corrosion behaviour of the Cu–35Ni–10Al alloy.

EIS measurements were performed at an open-circuit potential between 0.01 and 1×10^5 Hz using a Zahner (model Zennium) potentiostat. The amplitude of the input sine signal was 5 mV. The corroded samples were examined by scanning electron microscopy (SEM) coupled with energy dispersive X-ray (EDX) microanalysis.

3. RESULTS AND DISCUSSION

Fig. 3 shows the impedance plots for the corrosion of Cu-35Ni-10Al alloys with different immersion times in the molten salts. The impedance spectra are composed of a small semi-circle in the high-frequency region and a line in the low-frequency region, indicating that the corrosion was controlled by a mass transfer process (e.g., Warburg diffusion). The semi-circle in the high-frequency region is not evident over the total immersion time. With increasing immersion time, the values of |Z| decrease, which indicates an increase in the corrosion rate. Meanwhile, the decrease in the phase angle in the middle-frequency region with the increase in the immersion time also proves less coverage of the corrosion product on the surface of the alloys.
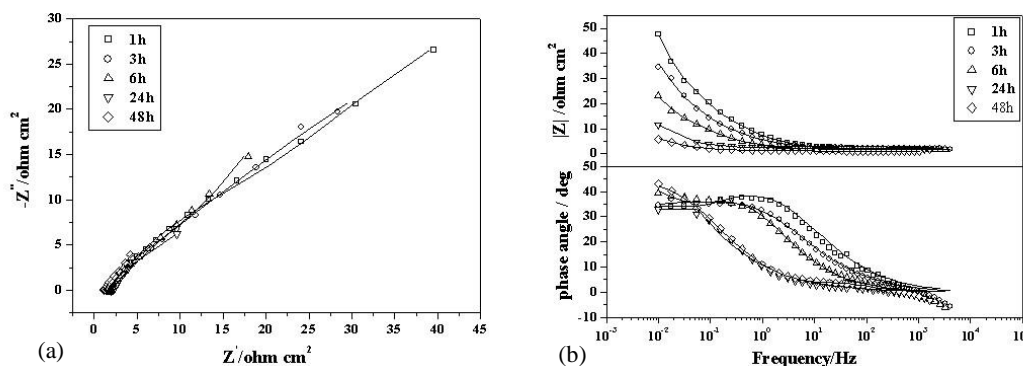

Figure 3. Nyquist plots (a) and Bode plots (b) of Cu–35Ni-10Al corroded in molten (0.62Li, 0.38K)$_2$CO$_3$ at 650°C in air for 1, 3, 6, 24, and 48 h. Symbol: experimental data and line: fitted data
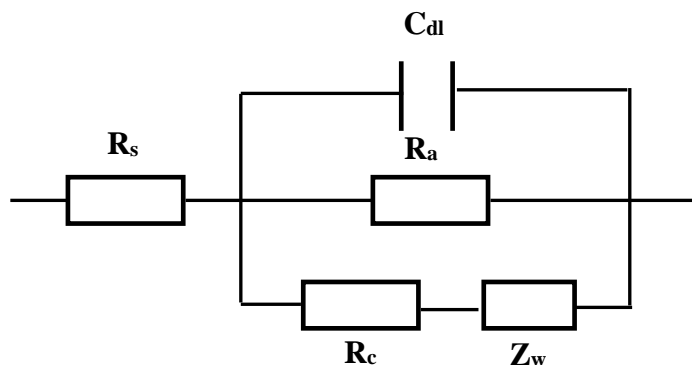

Figure 4. Equivalent circuits representing the corrosion of Cu–35Ni-10Al in molten (0.62Li, 0.38K)$_2$CO$_3$ at 650°C in air

As a porous scale forms on an alloy surface, the anodic and cathodic charge transfers are not the rate limiting steps. The corrosion will be controlled by the diffusion of oxidants in the melt. An equivalent circuit (as shown in Fig. 4) is used to describe the impedance spectroscopy result for the corrosion of an alloy, where R_s represents the molten-salt resistance, C_{dl} the double-layer capacitance, R_a the anodic charge-transfer resistance, R_c the cathodic charge-transfer resistance, and Z_w the diffusion-induced Warburg resistance.

The electrochemical impedance for the circuit in Fig. 4 can be expressed by Eq. (1) [14]. The Warburg resistance Zw may be expressed by Eq. (2).

$$Z = R_s + \cfrac{1}{jC_{dl}\omega + C_{dl}\omega\cot(\beta\pi/2) + \cfrac{1}{R_a}\omega + \cfrac{1}{R_c + Z_w}} \tag{1}$$

$$Z_w = A_w(j\omega)^{N_w} \tag{2}$$

Where A_w is the modulus of the Warburg resistance associated with the solubility and diffusion coefficient of the oxidants in the melt; and N_w is the Warburg coefficient, $0.5 \langle\!\langle N_w < 0$. According to Eqs. (1) and (2), it can be seen that R_c is much greater than Z_w at high frequency. Thus, Eq. (2) may be simplified to Eq. (3):

$$Z = R_s + \cfrac{1}{jC_{dl}\omega + C_{dl}\omega\cot(\beta\pi/2) + \cfrac{1}{R_a}\omega + \cfrac{1}{R_c}} \tag{3}$$

where $R_t = (R_a R_c)/(R_a + R_C)$ represents the charge transfer resistance. The fitted results are listed in Table 1. The value of R_t decreases as the immersion time increases, indicating an increase in the corrosion rate in the melt. Moreover, the deviation of β from 1 indicates a dispersion effect, which is a notable feature of molten salt corrosion.

Table 1. Fitting results for the impedance spectroscopy results of Cu–35Ni-10Al during corrosion in melts

Time (h)	R_s ($\Omega.cm^2$)	C_{dl} ($S^{-\alpha}\Omega^{-1}cm^{-2}$)	R_t ($\Omega.cm^2$)	β
1	1.743	0.0512	48.71	0.596
6	2.005	0.0750	33.26	0.5957
24	2.021	0.3221	25.36	0.6477
48	1.091	0.1083	10.44	0.7580

Fig. 5 shows the cross-sectional morphology of Cu-35Ni-10Al corroded in the melt for 48 h. The corrosion products are porous, layered and composed of a sequence of bright and black regions. The distribution of the Cu-rich phase (bright zone) and Ni-Al-rich phase (dark zone) in the original alloy is maintained. From the analysis of the SEM images and EDS results, the bright zone is the Cu-Ni oxide phase (point 1). The grey regions are a mixture of Al-rich oxides (point 2), and the black products are mainly Ni–Al–rich oxides (point 3). The corrosion in the Cu-rich zone is more rapid than that in the Ni-Al-rich zone, and obvious holes exist on the scale.
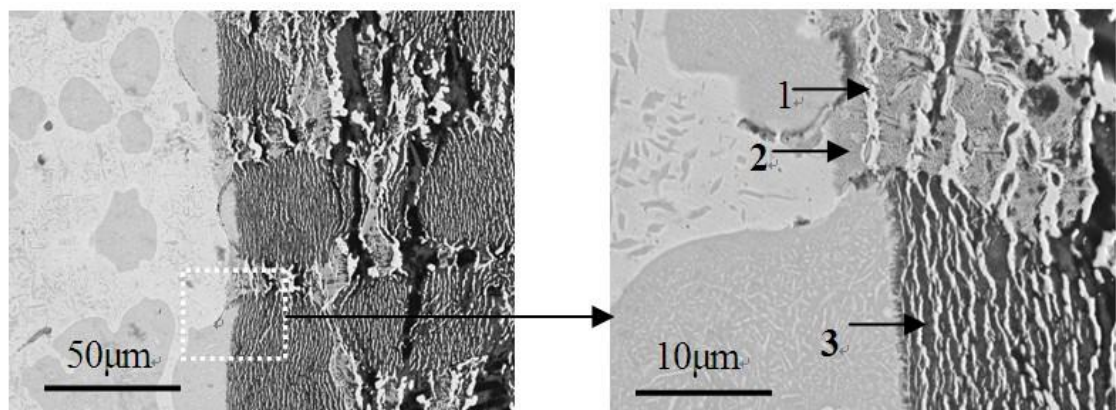
Figure 5. Cross-sectional morphology of Cu-35Ni-10Al corroded in molten $(0.62Li, 0.38K)_2CO_3$ at 650°C in air for 48 h.

Zeng [15] reported that a two-phase Cu-15Al alloy immersed in molten carbonate at 650°C could form a continuous and protective Al_2O_3 scale. For a Cu-Al alloy, 5% (mass fraction) Al can form protective Al_2O_3 at high temperature[16]. However, the addition of Ni in an alloy decreases the Al diffusion rate in the bulk[17]. In this work, the corrosive species in the melts are apt to penetrate the corrosion product and form a porous scale. In the carbonate molten melt, O_2^{2-} and O_2^- form by the combination of O_2 with CO_3^{2-} at the melt/gas interface and diffuse to the scale/melt interface[15]. Additionally, as illustrated in Figure 3, the impedance response for the corrosion of the alloys shows a typical diffusion character. As mentioned above, the diffusion of O_2^{2-} and O_2^- is the rate-limiting step for the corrosion of Cu-35Ni-10Al alloy in the melts. Because low valence Cu_2O in the inner scale can quickly react with O_2^{2-} or O_2-producing O_2, the faster diffusion of oxygen along the copper-oxide interface promotes internal oxidation and accelerates alloy corrosion with the extended immersion time. Thus, it could be observed that the corrosion in the Cu-rich zone was faster than that in the Ni-Al-rich zone for Cu-Ni-Al alloy, as shown in Fig. 5. Similar results have also been observed in other alloy systems[18]. Additionally, the internal oxidation increases the volume scale and induces mechanical stresses. The stresses can produce a high density of defects and provide preferential paths for the diffusion of corrosive species.

In general, a continuous and protective Al_2O_3 film on the surface of an alloy is the most critical factor for the potential application of Cu-Ni-Al alloy as an anode material for MCFCs. To enhance the corrosion resistance of Cu-Ni-Al alloys at high temperature in molten carbonate, the influence of the composition and microstructure on the growth mechanism of the oxide layer on the Cu-Ni-Al alloys still needs further investigation.

4. CONCLUSIONS

The corrosion behaviour of cast Cu-35Ni-10Al alloy in molten $(0.62Li, 0.38K)_2CO_3$ at 650°C was investigated by electrochemical impedance spectroscopy (EIS). After immersion in the melt for 48 h, a porous and layered scale formed on the Cu-35Ni-10Al alloy surface. The electrochemical impedance

spectroscopy results for the corrosion of Cu-35Ni-10Al in molten (Li, K)$_2$CO$_3$ at 650°C showed a small semi-circle at high frequency and a line at low frequency, which are typical of a diffusion-controlled corrosion process. The values of R$_t$ decreased with the immersion time, suggesting an enhanced corrosion rate. The faster internal oxidation is responsible for the accelerated corrosion of Cu-35Ni-10Al in the melt.

References

1. J.H. Wee, D.J. Song, C.S. Jun, T.H. Lim, S.A. Hong, H.C. Lim, K.Y. Lee, *J. Alloys. Comp,*390(2005)155.
2. J.H. Wee, *Mater. Chem. Phys*, 98(2006)273.
3. G. Özkan，U.C. İyidir, *Energy Source Part A,* 37(2015)2487.
4. H. Numata, O. Nakasaki, I. Ohno and S. Haruyama, *Zairyo-to-Kankyo*, 40(1991)110.
5. E.R. Hwang, S.G. Kang,*J. Power Sources*, 76(1998)48.
6. E.R. Hwang, J.W.Park, Y.D.Kim, S.J.Kim, S.G. Kang,*J. Power Sources*.69(1997)55.
7. C.Li, J. Chen, W. Li, Y.L Hu, Y.J. Ren, W.Qiu, J.J. He, J.L.Chen, *Mater. Sci-Poland*, 32(2014)341.
8. W. Li, H. Liang, J. Chen, J.W. Yang, X.Z. Li, *Chin. J. Mech. Eng,* 2(2015)58
9. C.S. Ni, L.Y. Lu, C.L. Zeng ,Y. Niu, *Corros.Sci*, 53(2011)1018.
10. L. Liu, Y. Li, C.L. Zeng, F.H.Wang, *Electrochim. Acta*, 51(2006)4736.
11. E. M. Zahrani , A.M. Alfantazi, *Corros.Sci*, 65(2012)340.
12. M. Zhu, S. Zeng, H.H. Zhang, J.Y. Li, B.Y. Cao,*Sol.Energy Mater. Sol. Cells,*186 (2018) 200.
13. J. Chen, Z. H. Huang, Y. J. Ren, J.L.Chen, J.J.He, *High Temp. Mat. Pr*, 32(2013)581.
14. C. L. Zeng, W. Wang and W. T. Wu,*Oxid. Met*, 53(2010)289.
15. C.L. Zeng, P.Y. Guo and W.T. Wu, *Electrochimica Acta*, 49(2004)1445.
16. Z.Q.Cao, L.Yu, K. Zhang, *J.Alloys. Comp*, 480(2009)449.
17. J.H.Xiang, Y.Niu, W.T.Wu, *Rare Metal. Mat. Eng*, 33(2004)1104.
18. C.L.Zeng, P.Y.Guo, W.T.Wu, *Electrochimica Acta*, 49(2004)2271.